

A probabilistic creep model incorporating test condition, initial damage, and material property uncertainty

Md Abir Hossain^{*}, Calvin M. Stewart

Department of Mechanical Engineering, The University of Texas at El Paso, 500 West University Avenue, Suite A126, El Paso, TX, 79968-0521, USA



ARTICLE INFO

Keywords:

Anderson-darling test
ANOVA
Coefficient of variation test
Lifetime prediction
Monte Carlo methods

ABSTRACT

Uncertainty is prevalent in the creep resistance of alloys, where at elevated temperature and low pressure, rupture can range across logarithmic decades. In this study, a probabilistic continuum-damage-mechanics (CDM)-based model is derived to capture the uncertainty of creep resistance. To meet this objective, creep data for alloy 304 Stainless Steel is gathered. A constitutive model, "Sinh", is calibrated deterministically to determine the statistical variability of the material properties. Three sources of uncertainty are injected into the model: test condition (stress and temperature), initial damage, and material properties. Probabilistic simulations are carried out by (a) calibrating probability distribution functions (pdfs) for each source of uncertainty (b) randomly sampling the pdfs using Monte Carlo methods and (c) executing simulations to replicate the uncertain creep behavior. A sensitivity analysis is performed to evaluate the relative effect of each source of uncertainty. In full probabilistic simulations, the cumulative uncertainty of creep behavior is evaluated. The probabilistic model accurately predicts the creep deformation and rupture of the available experiments. The probabilistic model is validated for interpolation but lacks extrapolation ability. Several future works are proposed to further improve the model.

1. Introduction

1.1. Motivation

Creep is a stress, temperature, and time-dependent phenomenon that exhibits considerable uncertainty. Long-term stress-rupture data can exhibit uncertainty spanning logarithmic decades. It is difficult to elucidate the service life of a long-lived component without extensive experimentation, reliability analysis, and inflated safety factors. The origin of the uncertainty in the creep data stems from many sources; notably, test conditions, service conditions, metallurgical inhomogeneities (due to thermomechanical processing, prior service, surface, and subsurface defects), geometric parameters, and test procedure error [1–4]. These sources of uncertainty in the creep data should be integrated into a probabilistic modeling approach to enable a more reliable prediction of creep deformation, damage evolution, and rupture in structures.

1.2. Uncertainty in creep data

Uncertainty is readily observed in the creep rupture data of most alloys as scatter [5,6]. The amount of scattering is dependent on alloy (i.e., chemical composition) and product form (bar, plate, tube, pipe, etc.) and can vary by order of magnitude [7]. A single alloy can exhibit a staggering range of uncertainty (4000 to 100,000 h) when multiple heats are aggregated and compared [8]. Uncertainty persists in other creep properties. The coefficient of variation (CoV) of accumulated-primary-creep-strain, minimum-creep-strain-rate, and creep ductility properties are two to three times higher than those observed in creep rupture data [9].

Efforts have been made to experimentally identify the sources of uncertainty in creep data [10]. Temperature fluctuations are unavoidable during long-term creep testing. Hayhurst observed a small temperature variation of ± 3 °C corresponds to a $\pm 8\%$ variation in creep rupture of silicon-killed 0.3–1.5%Mg steels [11]. Specimens are machined to a tight tolerance; however, a small eccentricity of 1.5% (which adds normal bending stress) can reduce creep rupture by over 60% depending on alloy and test conditions. Farris measured the eccentricity of Copper-bicrystals specimen and found that eccentricity has

* Corresponding author.

E-mail address: mhossain9@miners.utep.edu (M.A. Hossain).

| Nomenclature | |
|--|---|
| $\dot{\epsilon}_{cr}$ | Creep strain rate |
| $\dot{\epsilon}_{final}, \dot{\epsilon}_{min}$ | Final- and minimum-creep-strain-rate |
| ϵ_{pr} | Primary creep strain |
| $\dot{\omega}$ | Damage rate |
| ω_0 | Initial damage |
| ω^* | Analytical damage |
| $\dot{\omega}_{final}, \dot{\omega}_{min}$ | Final- and minimum-damage-rate |
| A, σ_s | Secondary creep constant |
| λ | Creep strain trajectory constant |
| φ | Damage trajectory constant |
| M, σ_t, χ | Rupture constants |
| A^* | Specimen-specific secondary creep constant |
| M^* | Specimen-specific rupture constant |
| Q_c | Apparent activation energy |
| t_r | Rupture time |
| $\sigma_{max}, \sigma_{min}$ | Maximum and minimum normal bending stress |
| F | Applied force |
| t | Tolerance of dimension relative to neutral axis |
| e | Eccentricity of the loading |
| T_i | Temperature recorded from thermocouple |
| AD | Anderson-Darling test |
| CDM | Continuum-damage-mechanics |
| CI | Confidence interval |
| CSR | Creep strain rate |
| CoV | Coefficient of variation |
| KR | Kachanov-Rabotnov |
| MCSR | Minimum-creep-strain-rate |
| SCRI | Service condition creep rupture interference |
| SR | Stress-rupture |
| TTT | Time-temperature-transformation |
| TPP | Time-temperature-Precipitation |

a strong correlation to the CoV of stress-rupture data [12]; however, eccentricity could not fully account for the uncertainty observed in low-stress long-duration data suggesting additional sources of uncertainty. The microstructure of specimens is unique. Creep resistance is greatly influenced by microstructural evolution. Eggeler measured the cavitation parameters $A - , \rho - ,$ and A^* in micrographs of the failed specimen and determine that both the evolution of metallurgical inhomogeneities and the initial state of the microstructure play a role in the scatter observed in stress-rupture data [13]. These and other sources of uncertainty must be considered when developing a probabilistic model.

1.3. Probabilistic creep modeling

Creep constitutive models are often applied deterministically where scatter is not considered; rather, the best-line through the data is the target of calibration. Creep models such as MPC-Omega, Theta-projection, Wilshire, and Sine-hyperbolic (Sinh) are employed in this fashion [14–17]. Deterministic models can be converted into probabilistic models by injecting uncertainty into their formulation.

Several “single-source” uncertainty models have been developed [18–22]. Appalanaidu developed a stochastic creep damage growth model where temperature uncertainty is modeled using white noise functions [18]. It was determined that the choice of noise function has a significant impact on the scatter in damage predictions. Harlow et al. proposed a probabilistic Kachanov-Rabotnov CDM-based model where material property uncertainty is incorporated using probability distribution functions (pdfs) and exact relations from probability theory [19]. Hossain and Stewart developed a probabilistic CDM-based Sine-hyperbolic (Sinh) creep-damage model where material property uncertainty is added using normal distributions and Monte Carlo methods [20]. Appalanaidu et al. developed a stochastic finite element methodology for pipe where material properties are spatially uncertain (i.e., inhomogeneous) using 2-D non-Gaussian random fields [21]. Kim and colleagues employed four different probabilistic methods to add material property uncertainty into a creep-crack-growth-rate model (least square fitting method, mean value method, probabilistic distribution method, and Monte Carlo method) [22]. This study revealed the determination of parameter B and q for power law equation between creep-crack-growth-rate and C^* integral is best suited by the Monte Carlo method as this method is expected to achieve a more accurate and economically viable solution due to the inherent conservatism of the technique.

Other researchers have developed “multiple-source” of uncertainty

models [1,12,23–26]. Penny et al. proposed a stochastic Kachanov-Rabotnov (KR) CDM-based model where load and material uncertainties are modeled using Monte Carlo methods [23]. Farris performed probabilistic stress-rupture simulations that included temperature, stress, and eccentricity uncertainty using Monte Carlo methods [12]. The three uncertainties matched the scatter observed in short-term data but did not capture the full experimental uncertainty in long-term data suggesting additional sources. Bhattacharya et al. proposed a CDM-based model that encompasses several categories of material property uncertainty, microstructural damage evolution properties, critical damage, and macroscopic material properties [24]. It was concluded that the source of uncertainty and the type of probability distribution function (normal, uniform, lognormal) applied have a large influence on the scatter observed in predictions. Vojdani et al. developed a stochastic creep-fatigue crack propagation model that included geometric, material property, and operating condition uncertainty [1]. It was determined that a sensitivity analysis of the random parameters must be performed to elucidate the order of importance of the random variables. Kim and colleagues developed a service condition creep rupture interference (SCRI) model where both the cumulative uncertainty of test conditions and service conditions are considered in stress-rupture predictions [25,26]. Monte Carlo simulations showed a rapid decrease in reliability of stress-rupture at higher fluctuation of service stress and temperature.

1.4. Problem statement

Recently, the Sine-hyperbolic (Sinh) continuum-damage-mechanics (CDM)-based constitutive model has been established as a reliable deterministic model for creep deformation, damage, and rupture of various alloys [27–31]. Studies have been performed to evaluate the stress-sensitivity, mesh-dependence, and convergence of Sinh in comparison with other established models [28] as well as the calibration of Sinh using disparate data for the long-term prediction of creep behavior [29]. Recent studies suggest Sinh is a good platform for probabilistic creep modeling [20,31].

2. Objectives

To that end, the objective of this study is to develop a probabilistic Sinh model to predict the uncertainty of creep deformation, damage, and rupture in alloys. To meet this objective (a) a probabilistic calibration approach is needed, (b) a sensitivity analysis is needed to determine the extent that each source of uncertainty contributes to creep

resistance, (c) and the full probabilistic model must be validated against replicated creep data. To meet this objective, five-replicant creep test data for alloy 304 Stainless Steel is gathered from literature [9]. The Sinh model is calibrated deterministically, to calculate the statistical variability of specimen-specific material properties. A probabilistic framework is introduced where three sources of uncertainty: test conditions, initial damage, and material properties are converted into probability distribution functions (pdfs). The probability distribution functions are calibrated using the Anderson-darling (AD) goodness-of-fit test [32,33]. Monte Carlo simulations are employed to randomly sample the pdfs and generate probabilistic creep predictions. A sensitivity analysis using the analysis of variance (ANOVA) approach is employed to determine the relative effect of the sources. Full probabilistic predictions are performed to determine if the model can capture the experimental uncertainty observed in the data.

3. Sine-hyperbolic (Sinh) model

The Sine-hyperbolic (Sinh) CDM-based model was developed to model the secondary and tertiary creep regimes [27]. The temperature-dependent form of Sinh consists of a creep-strain-rate (CSR) and damage evolution equation as follows

$$\dot{\epsilon}_{cr} = A \exp\left(\frac{-Q_c}{RT}\right) \sinh\left(\frac{\sigma}{\sigma_s}\right) \exp(\lambda\omega) \quad (1)$$

$$\dot{\omega} = \frac{[1 - \exp(-\varphi)]}{\varphi} M \exp\left(\frac{-Q_c}{RT}\right) \sinh\left(\frac{\sigma}{\sigma_t}\right)^{\chi} \exp(\varphi\omega) \quad (2)$$

where σ is stress, T is temperature in Kelvin, R is the universal gas constant, Q_c is the apparent activation energy, A and σ_s are the secondary creep constants, λ is the strain trajectory constant, M , σ_t , and χ are rupture constants, φ is the damage trajectory constant, and ω is damage an internal state variable that evolves from an initial damage, ω_0 to unity [28]. These equations can be simplified for isothermal conditions by absorbing the term $\exp(-Q_c/RT)$ into the constants A and M .

Assume that initial damage is zero, $\omega_0 = 0$ at $t = 0$. The secondary creep material constants, A and σ_s , can be calibrated using the “temperature-normalized” minimum-creep-strain-rate (MCSR)

$$\frac{\dot{\epsilon}_{min}}{\exp\left(\frac{-Q_c}{RT}\right)} = A \sinh\left(\frac{\sigma}{\sigma_s}\right) \quad (3)$$

where the $\dot{\epsilon}_{min}$ is the minimum-creep-strain-rate (MCSR) measured from creep data. The activation energy, Q_c is obtained by maximizing the log-log square of the Pearson product moment correlation coefficient of a regression line through MCSR or stress-rupture (SR) data [34]. Stress-rupture (SR) data denotes the rupture time plotted versus stress.

The λ and φ constants exhibit stress and temperature dependence. The strain trajectory constants, λ is unitless and equal to

$$\lambda = \ln\left(\frac{\dot{\epsilon}_{final}}{\dot{\epsilon}_{min}}\right) \quad (4)$$

where $\dot{\epsilon}_{final}$ is the final-creep-strain-rate (FCSR) measured from creep data and $\lambda \geq 0$. The damage-trajectory constant φ is unitless and equal to

$$\varphi = \ln\left(\frac{\dot{\omega}_{final}}{\dot{\omega}_{min}}\right) \quad (5)$$

where the minimum-damage-rate, $\dot{\omega}_{min}$ and final-damage-rate, $\dot{\omega}_{final}$ are not experimentally measured but can be analytically calculated and $\varphi \geq 1$. Analytical damage, ω^* and damage rates, $\dot{\omega}^*$ data can be calculated from [Eq. (1)] and [Eq. (3)] as follows

$$\begin{aligned} \omega^* &= \frac{1}{\lambda} \ln\left(\frac{\dot{\epsilon}_{cr}}{\dot{\epsilon}_{min}}\right) \\ \dot{\omega}^* &= \frac{\Delta\omega^*}{\Delta t} \end{aligned} \quad (6)$$

Herein, the internal state variable damage, $\omega = 0$ at MCSR.

The creep strain trajectory constant, λ and damage trajectory constant, φ exhibit stress and temperature-dependence. The dependencies of λ and φ are modeled according to Eyring's equations [35,36].

$$\lambda(\sigma, T) = \lambda_0 \exp\left(-\frac{V_{\lambda}^* \sigma}{k_b T}\right) \quad (7)$$

$$\lambda \geq 0$$

$$\varphi(\sigma, T) = \varphi_0 \exp\left(\frac{V_{\varphi}^* \sigma}{k_b T}\right) \quad (8)$$

$$\varphi \geq 1$$

where λ_0 and φ_0 are unitless coefficients, V_{λ}^* and V_{φ}^* are the activation volume for λ and φ respectively, σ is stress, T is temperature, and k_b is the Boltzmann constant.

Integration of the damage evolution [Eq. (2)] furnishes damage, ω following CDM laws and the “temperature-normalized” rupture, t_r as follows

$$\omega(t) = -\frac{1}{\varphi} \ln\left[1 - [1 - \exp(-\varphi)] \frac{t}{t_r}\right] \quad (9)$$

$$t_r \exp\left(\frac{-Q_c}{RT}\right) = \left[M \sinh\left(\frac{\sigma}{\sigma_t}\right)^{\chi}\right]^{-1} \quad (10)$$

Damage [Eq. (9)] depends on the constant φ and rupture, t_r . Rupture [Eq. (10)] depends on the M , σ_t , and χ material constants.

Assume that initial damage is $\omega_0 > 0$. The “temperature-normalized” MCSR and rupture predictions are reintegrated as

$$\frac{\dot{\epsilon}_{min}}{\exp\left(\frac{-Q_c}{RT}\right)} = A \sinh\left(\frac{\sigma}{\sigma_s}\right) \exp(\lambda\omega_0) \quad (11)$$

$$t_r \exp\left(\frac{-Q_c}{RT}\right) = \frac{[\exp(-\varphi) - \exp(-\varphi\omega_0)]}{M \sinh\left(\frac{\sigma}{\sigma_t}\right)^{\chi} [\exp(-\varphi) - 1]} \quad (12)$$

where the presence of initial damage will cause the MCSR to increase and rupture time to decrease. Damage with initial damage is also furnished as

$$\omega(t) = -\frac{1}{\varphi} \ln\left[\exp(-\varphi\omega_0) - [\exp(-\varphi\omega_0) - \exp(-\varphi)] \frac{t}{t_r}\right] \quad (13)$$

where the presence of initial damage causes the damage to increase.

A closed-form creep strain equation can be derived by combining [Eq. (1)] and [Eq. (9)] and performing definite integration as follows

$$\epsilon_{cr} = \frac{A \exp\left(\frac{-Q_c}{RT}\right) \varphi \sinh\left(\frac{\sigma}{\sigma_s}\right)}{(\lambda - \varphi)} \left[\frac{t_r}{\exp(-\varphi) - 1} - \frac{t + \frac{t_r}{\exp(-\varphi) - 1}}{\left(\frac{t_r - t + t \exp(-\varphi)}{t_r}\right)^{\frac{1}{\varphi}}} \right] \quad (14)$$

where initial damage can be added by inserting [Eq. (12)].

4. Material

Creep data for alloy 304 stainless steel (304SS) bar was gathered from literature [9]. The chemical composition (wt%) of the alloy 304SS

Table 1

Chemical composition (wt%) of 304SS [9].

| C | Si | Mn | P | S | Ni | Cr | Mo | Cu | N |
|------|------|------|-------|-------|------|-------|------|------|-------|
| 0.02 | 0.40 | 1.83 | 0.029 | 0.009 | 8.13 | 18.22 | 0.24 | 2.06 | 0.102 |

Table 2

Statistical uncertainty of MCSR and rupture of replicated creep tests [9].

| Temperature, T (°C) | Stress, σ (MPa) | MCSR, $\dot{\varepsilon}_{\min}$ | | | Rupture, t_r | | |
|--------------------------|---------------------------|----------------------------------|------------------------------|------------|----------------|-------------|------------|
| | | Max (%·hr ⁻¹) | Min (%·hr ⁻¹) | CoV (%) | Max (hr) | Min (hr) | CoV (%) |
| 600 | 320 | 0.072 | 0.029 | 34.57 | 147.43 | 100.00 | 16.12 |
| 600 | 300 | 0.025 | 0.011 | 34.95 | 63.36 | 46.05 | 12.55 |
| 650 | 260 | 0.188 | 0.108 | 23.33 | 42.12 | 26.88 | 16.60 |
| 650 | 240 | 0.461 | 0.017 | 48.02 | 163.52 | 127.61 | 9.48 |
| 700 | 180 | 0.056 | 0.020 | 43.02 | 93.12 | 82.73 | 4.48 |
| 700 | 160 | 0.008 | 0.006 | 12.74 | 196.41 | 156.95 | 8.79 |

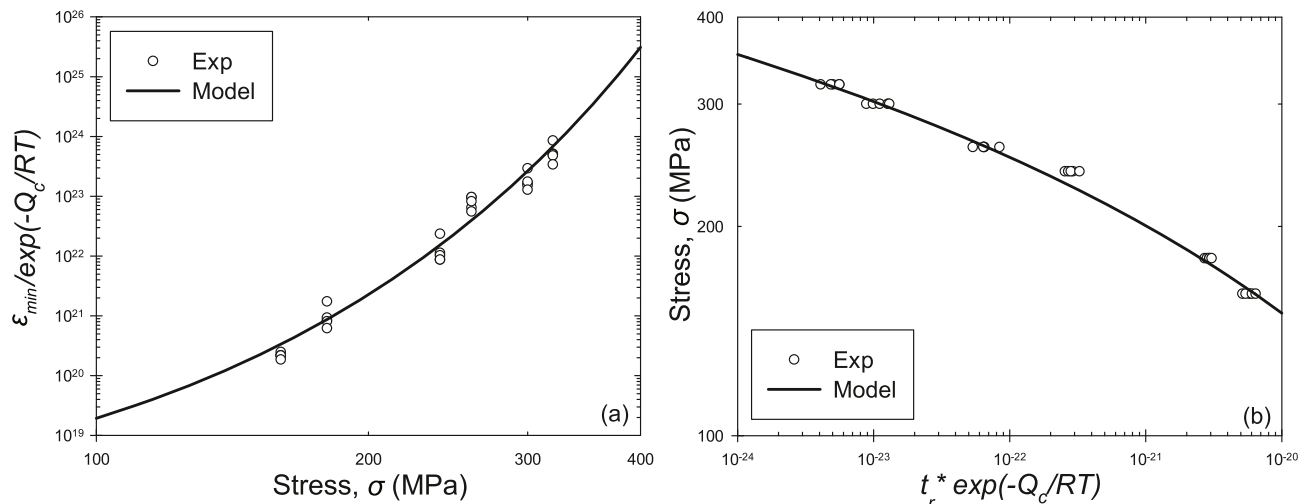


Fig. 1. Normalized (a) MCSR and (b) SR data with deterministic calibration using [Eqs. (3)–(10)].

is listed in **Table 1**. The room temperature tensile strength, yield strength, and elongation are 706 MPa, 490 MPa, and 18% respectively. The 6 mm gauge diameter and 30 mm gauge length specimens were fabricated from 20 mm diameter bar and experiments are carried out according to ASTM E139 standard [37].

A total of thirty creep curves were collected with tests conducted in quintuplicate (five repeats). The test conditions, minimum-creep-strain-rate (MCSR), and rupture data are provided in **Table 2**. The creep data exhibits scatter. Coefficients of variations (CoV) up to 48% and 16% are observed in the MCSR and rupture data, respectively.

5. Results and discussion

5.1. Deterministic calibration

Nine material constants are required for the Sinh model: four are fixed ($Q_c, \sigma_s, \sigma_t, \chi$) and five are specimen-specific ($\varepsilon_{pr}, A^*, M^*, \lambda, \varphi$) [29]. The stress and temperature sensitivity controls the selection of fixed and specimen-specific material constants. The normalized MCSR and SR data are plotted in **Fig. 1**. The normalized data exhibits appreciable scatter. The scattering is evident by the CoV statistics of MCSR and SR as summarized in **Table 2**. The normalized MCSR and SR [Eqs. (3)–(10)] are calibrated to best-fit the experimental data resulting in the fixed

material constants listed in **Table 3**. Note, best-fit A and M were also obtained and will be employed later in the probabilistic model. The activation energy, Q_c is comparable to literature [38]. Specimen-specific material constants are calculated to produce best-fit predictions of the MCSR, SR, and creep ductility specific to each creep curve. The A^* and M^* constants are back-calculated from [Eqs. (7) and (8)]. The λ constant is calculated from the MCSR and FCSR data using [Eq. (4)]. The specimen-specific material constant φ is numerically optimized using the closed-form creep strain [Eq. (14)] equation. The specimen-specific primary creep strain, ε_{pr} is measured directly from creep data. The

Table 3

Fixed material constants for Sinh model of alloy 304SS

| Q_c (kJ·mol ⁻¹) | A (%·hr ⁻¹ × 10 ¹⁷) | σ_s (MPa) | M (hr ⁻¹ × 10 ¹⁷) | σ_t (MPa) | χ |
|----------------------------------|---|---------------------|---|---------------------|--------|
| 419 | 3.310 | 21 | 9.462 | 66.5 | 3.0 |

*these are temporary material constants that best-fit the SR and MCSR data. The specimen-specific constants (specific to each creep curve) are provided in the Appendix **Table 8**.

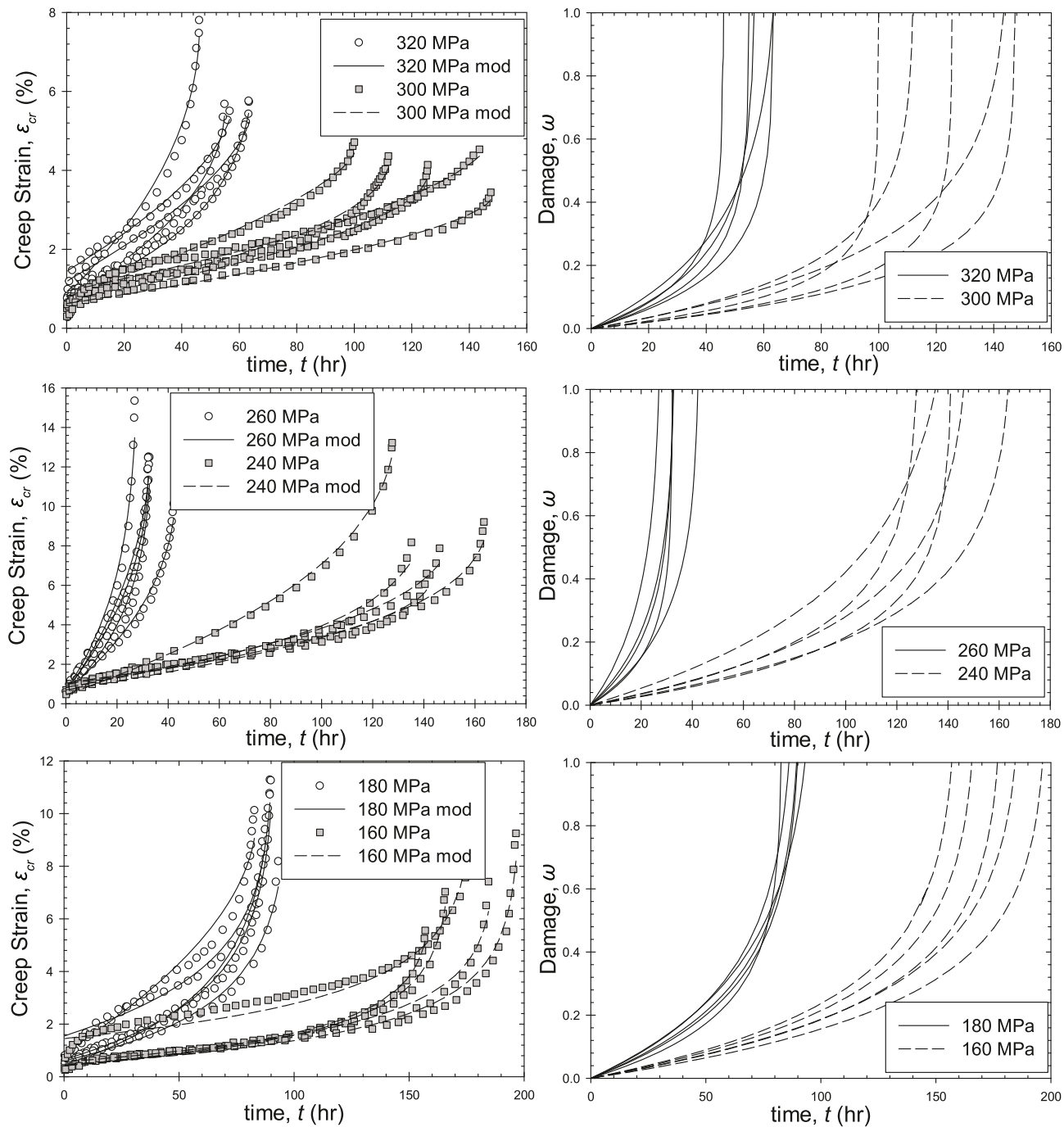


Fig. 2. Deterministic creep deformation and damage predictions using the Sinh model for 304SS (a) 600 °C at 300 and 320 MPa, (b) 650 °C at 260 and 240 MPa, and (c) 700 °C at 180 and 160 MPa.

specimen-specific material constants for all thirty creep curves are provided in Table 8 of the Appendix.

The creep deformation and damage predictions using the specimen-specific constants are shown in Fig. 2. Qualitatively and quantitatively, the model is highly accurate. The mean error in MCSR, SR, and creep ductility are 10.433, 0.0, and 8.978%, respectively. Critical damage is always unity. These deterministic predictions represent the case where uncertainty is carried 100% by the specimen-specific material properties. In the following section, the uncertainties will be distributed in a more realistic and systematic manner.

5.2. Probabilistic calibration

The probabilistic calibration process and model employ the closed-form Sinh equations with initial damage [Eqs. (11)-(13)]. The previously determined fixed material constants ($Q_c, A, \sigma_s, M, \sigma_t$) are preserved. Scatter in the experimental data is captured by defining probability distribution functions (pdfs) for the test conditions (σ and T), initial damage, ω_0 , and material constant ($\epsilon_{pr}, \lambda, \varphi$) uncertainty. Note, these uncertainties are not co-calibrated; rather, they are individually calibrated and allowed to naturally converge/interfere in the full probabilistic model. The calibrated pdfs are shown in Fig. 3 and their parameters are summarized in Table 4. The Anderson-darling (AD)

goodness-of-fit test was employed to identify and calibrate the pdfs. The probabilistic parameters conform to ASTM standards, CDM rules, and the nature of the specimen-specific constants. A monograph of the calibration process follows.

Test condition uncertainties are idealized in Fig. 4. Test condition uncertainty can be calibrated by measuring the eccentricity of the specimen/load-frame and examining thermocouple data. In this study, that information is not available; therefore, to be conservative, the worst-case scenario allowed under ASTM standards is applied. Stress

fluctuations arise from the eccentric loading of a specimen due to the misalignment of the load-frame and/or dimensional tolerance as illustrated in Fig. 4(a). The ASTM E8 standard calls for a stress increase of 1.5, 2.5, and 3.2% for 12.5, 9, and 6 mm diameter specimens respectively when eccentricity is held to 0.025 mm [39]. In this study, the specimens have a diameter of 6 ± 0.025 mm, thus the worst-case scenario is +3.2% stress. Stress uncertainty is applied using Normal Gaussian pdf where the mean is equal to nominal stress and the standard deviation is equal to 1/4th of the linear function provided in Table 4.

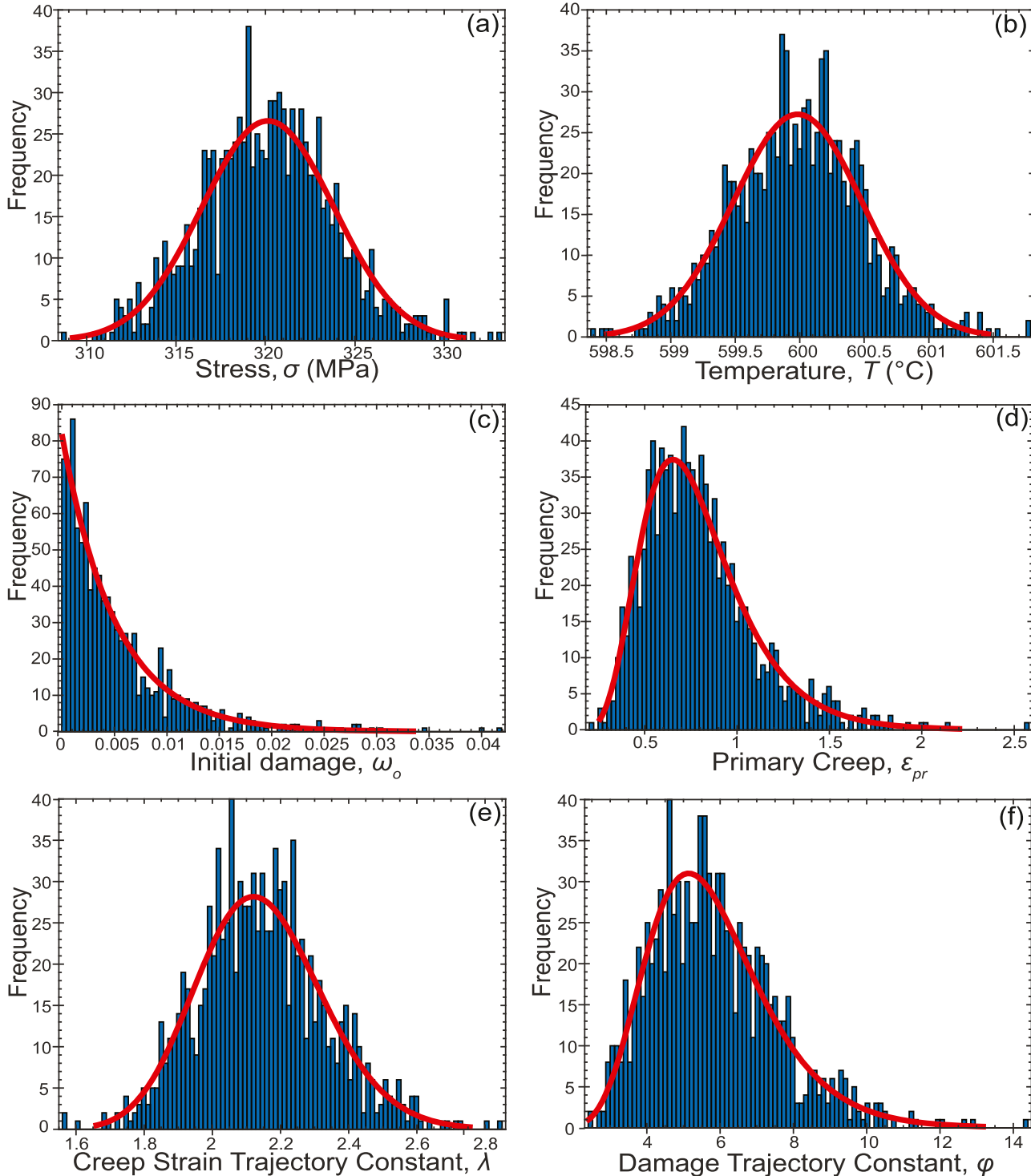
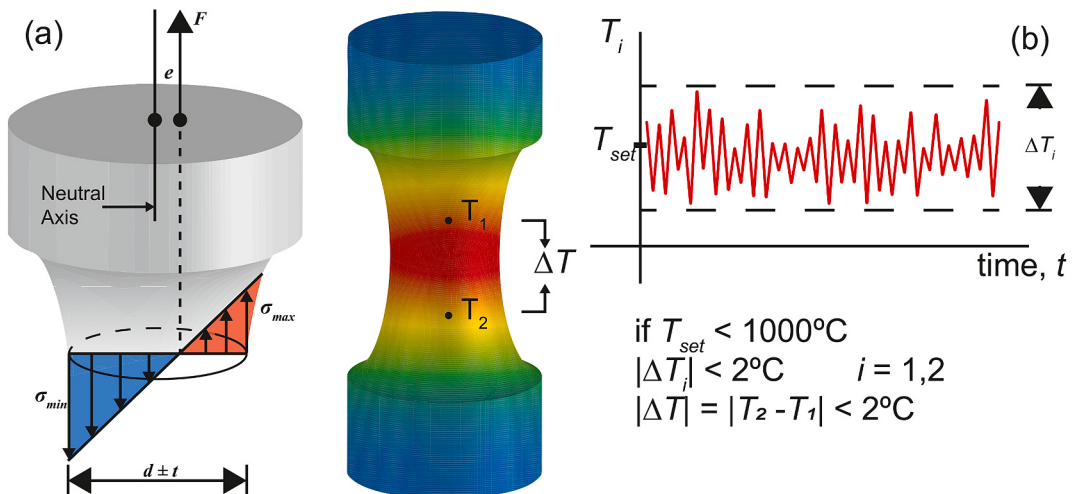


Fig. 3. Probability distribution functions (pdfs) for (a) stress, σ (b) temperature, T (c) initial damage, ω_0 (d) primary creep strain, ε_{pr} (e) creep strain trajectory constant, λ , and (f) damage trajectory constant, φ . These set of pdfs are for case 320 MPa at 600 °C.

Table 4

Probability distribution function type and parameters for probabilistic Sinh model.

| Uncertainty Parameter | Type of Distribution | PDF Parameters |
|-----------------------|----------------------|--|
| σ | Normal Gaussian | $\mu = X \text{ MPa}^a, \sigma = (0.046 \times X + 0.006)/4 \text{ MPa}$ |
| T | Normal Gaussian | $\mu = X^\circ\text{C}^a, \sigma = 4^\circ\text{C}/8$ |
| ω_0 | Exponential | $\mu = 0.005$ |
| ε_{pr} | Lognormal | $\mu = -0.309, \sigma = 0.362$ |
| λ_0 | Lognormal | $\mu = 1.664, \sigma = 0.084$ |
| φ_0 | Lognormal | $\mu = 0.971, \sigma = 0.289$ |

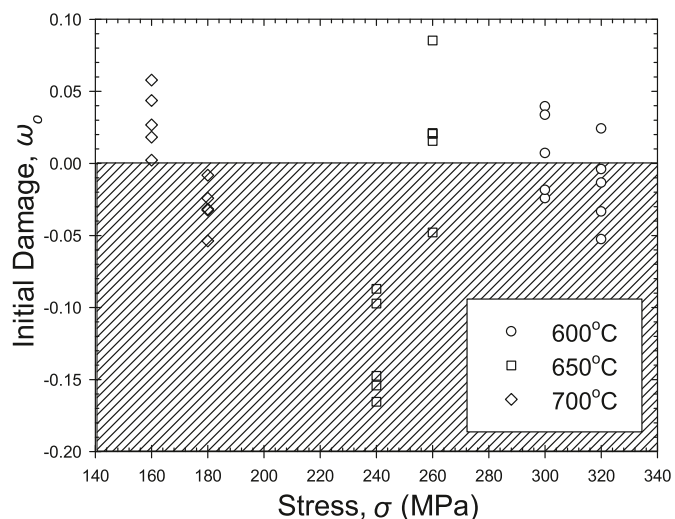
^a Where X is the nominal stress/temperature of interest.**Fig. 4.** Illustration of (a) eccentric loading and (b) temperature fluctuations during a creep test. Herein, $\sigma_{max}, \sigma_{min}$ - Maximum and minimum normal bending stress, F - Applied load, t - tolerance in dimensions relative to neutral axis, e - eccentricity of loading, and T_i - Temperature recorded from thermocouple.

The pdf for stress uncertainty is plotted in Fig. 3(a). The chosen pdf is appropriate because more than 95% of the distribution is captured within the $\pm 3.2\% \sigma$ bands. A more elaborate formula for adding stress uncertainty could be derived by using solid mechanics to solve for the stress increase caused by the interaction of load/geometric eccentricity, concentricity of the specimen gauge section and the load-frame, and load-frame misalignment as illustrated in Fig. 4. This necessary information is not available for the current study.

Temperature fluctuations arise during creep testing and exhibit both spatial (along with the specimen gauge-length) and temporal properties as illustrated in Fig. 4(b). The ASTM E139 standard states that temperature must not fluctuate more than $\pm 2^\circ\text{C}$ below 1000°C and $\pm 3^\circ\text{C}$ above 1000°C duration of testing [37]. Furthermore, since two thermocouples are required, fluctuations must remain below this limit at each location and between them, respectively. In this study, the specimens are subjected to temperatures below 1000°C , thus the worst-case scenario is $\pm 2^\circ\text{C}$ temperature. Temperature uncertainty is applied using a Normal Gaussian pdf where the mean is equal to nominal temperature and the standard deviation is equal to 1/8th of the temperature range as shown in Fig. 3(b). The chosen pdf is appropriate because 100% of the distribution is captured within the $\pm 2^\circ\text{C}$ bands.

Initial damage, ω_0 is influenced by residual stresses [24], pre-existing cavities and defects, and loading history including the monotonic loading need to reach the creep load [40–46]. Rather than evaluate these sub-sources of damage uncertainty, a collective approach is applied where the remaining uncertainty in the SR data is eliminated by adding initial damage. Initial damage, ω_0 is obtained by applying the specimen-specific φ constants (that were obtained when $\omega_0 = 0$) and rearranging the rupture equation [Eq. (12)] to solve for initial damage.

The resulting initial damage, ω_0 versus stress is plotted in Fig. 5. No stress- or temperature-dependence is observed. Positive ($n = 13$) and negative ($n = 17$) initial damage values are calculated. Negative initial damage, $\omega_0 < 0$ violates CDM and are therefore discarded [47]. Discarding $\omega_0 < 0$, the average ω_0 is 0.01. Initial damage uncertainty is applied using an exponential pdf with a mean $\mu = 0.005$ as plotted in Fig. 3(c). An exponential pdf is appropriate because the specimens are

**Fig. 5.** Initial damage, ω_0 versus stress calculated employing the specimen-specific λ and φ to obtain specimen-specific ω_0 from the SR data.

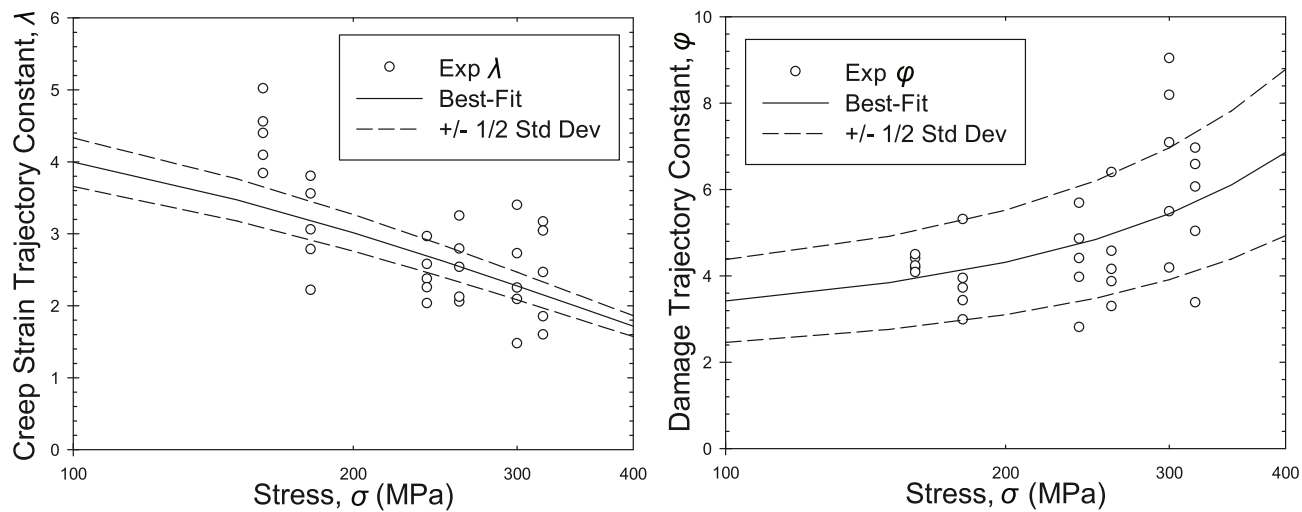


Fig. 6. Eyring's predictions [Eqs. (7) and (8)] of the specimen-specific constant λ and φ versus stress. The solid line is the best fit. The dashed lines represent best fit $\pm 1/2$ standard deviation.

Table 5
Eyring's constants for λ and φ .

| Parameter | Coefficient | Activation Volume (10^{-23}cm^3) |
|---------------------|-------------|---|
| λ [Eq. (7)] | 5.295 | 3.392 |
| φ [Eq. (8)] | 2.715 | 2.795 |

virgin with initial damage consisting of mostly pre-existing microstructural defects. Densitometry techniques can also be employed to estimate initial damage by measuring the bulk porosity and/or the local void volume fraction within the microstructure before testing [44–46].

The uncertainty of ε_{pr} is based on the specimen-specific values. The estimated ε_{pr} does not trend with stress or temperature. Uncertainty of ε_{pr} is applied using a Lognormal pdf where the mean and standard deviation are equal to -0.309 and 0.362 respectively as shown in Fig. 3(d). The Anderson-Darling (AD) goodness-of-fit test were employed to identify and calibrate the pdf. In the future, a multistage Sinh model could be employed [47]. The multistage Sinh allows explicit modeling of primary, secondary, and tertiary creep regimes.

The uncertainty of λ and φ is established based on the specimen-specific constants. Eyring predictions [Eqs. (7) and (8)] of λ and φ are plotted versus stress in Fig. 6. Best-fits are obtained by numerically optimizing the coefficients (λ_0 and φ_0) and activation volumes (V_λ^* and V_φ^*) as reported in Table 5. The standard deviation of the specimen-specific λ and φ are 0.892 and 1.523 respectively. The dashed lines are obtained by taking the best-fit coefficients (λ_0 and φ_0) $\pm 1/2$ standard deviation. The uncertainty is added to coefficients λ_0 and φ_0 using a Lognormal distribution as shown in Fig. 3(e)–(f), respectively. The activation volumes (V_λ^* and V_φ^*) remain fixed. The pdfs were selected based on Anderson-Darling (AD) goodness-of-fit test.

5.3. Monte Carlo sampling

A subroutine is developed to generate the probabilistic predictions. The flowchart is illustrated in Fig. 7. The global inputs of the subroutine are the fixed material constants ($Q_c, A, \sigma_s, M, \sigma_t$) in Table 3 and Eyring constants reported in Table 5, respectively. Monte Carlo sampling is applied to the $(\sigma, T, \varepsilon_{pr}, \omega_0, \varphi_0, \lambda_0)$ pdfs reported in Table 4 to generate 1000 unique creep deformation and damage curves per creep test. A coefficient of variation (CoV) convergence test is performed to determine the appropriate number of Monte Carlo samples as shown in Fig. 8

[48]. The creep ductility and rupture time converge in less than 400 samples. A sample size of 1000 is clearly adequate for this study.

5.4. Sensitivity analysis

A sensitivity analysis is performed by “turning on” each source of uncertainty individually. For brevity, only the creep deformation and damage predictions corresponding to the 320 MPa and 600 °C creep data are shown. Creep deformation predictions are provided in Fig. 9 (a–f). The black solid line is where temperature and stress are exact, and initial damage is zero. It is observed that each uncertainty parameter contributes differently to the creep deformation curve. These contributions arise naturally due to the mathematical form of the constitutive equations (i.e. location of the parameters within the equations) and the pdf applied to the parameter. Generally, the expected trends are observed for stress, temperature, initial damage, and primary creep strain uncertainty [49,50]. It is observed that temperature uncertainty makes no contribution to creep ductility. This can be attributed to the mathematical form of creep strain [Eq. (14)]. A mathematical exercise of creep strain [Eq. (14)] combined with rupture [Eq. (10)] determined that temperature alone does not change creep ductility; rather the temperature-dependence of λ and φ in Eyring's form [Eqs. (7) and (8)] control creep ductility. Overall, λ and φ contributed the most to creep ductility which may explain the large uncertainty in the calibrated values observed in Fig. 6. Increasing the creep strain trajectory constant, λ increases creep ductility without altering rupture time as shown in Fig. 9(e). Empirically, λ arises from the final-creep-strain rate [Eq. (4)], and subsequently correlates well to creep ductility. Increasing the damage trajectory constant, φ decreases creep ductility greatly and rupture time slightly as shown in Fig. 9(f). The material constant, φ accelerates the damage rate leading to a decrease in creep ductility and rupture time.

The damage evolution predictions are provided in Fig. 10(a–f). It is observed that the uncertainty parameters have differing contribution on damage evolution. Stress, temperature, initial damage, and primary creep contribute the expected behaviors [49,50]. The creep strain trajectory constant, λ , has no impact on damage evolution as shown in Fig. 10(e). This can be attributed to no mathematical relationship existing between λ and ω . The damage trajectory constant, φ shows the expected trends and sharpens the damage curve as shown in Fig. 10(f).

A quantitative analysis is performed on the uncertainty parameters using the analysis of variance (ANOVA) approach. The relative effect of each parameter on the MCSR, SR, and creep ductility is shown in Fig. 11. Relative effect (%) expresses the influence of one source relative to other

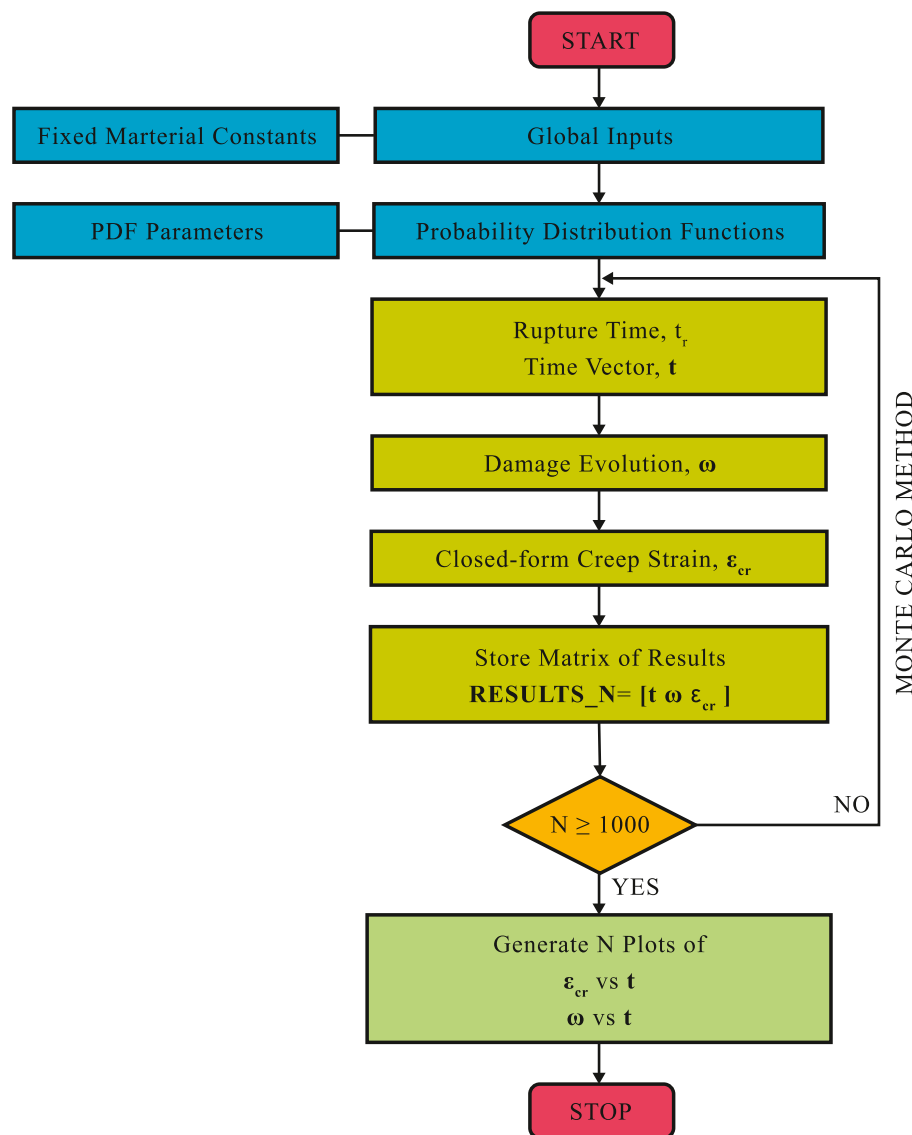


Fig. 7. Flowchart of probabilistic model using Monte Carlo sampling method.

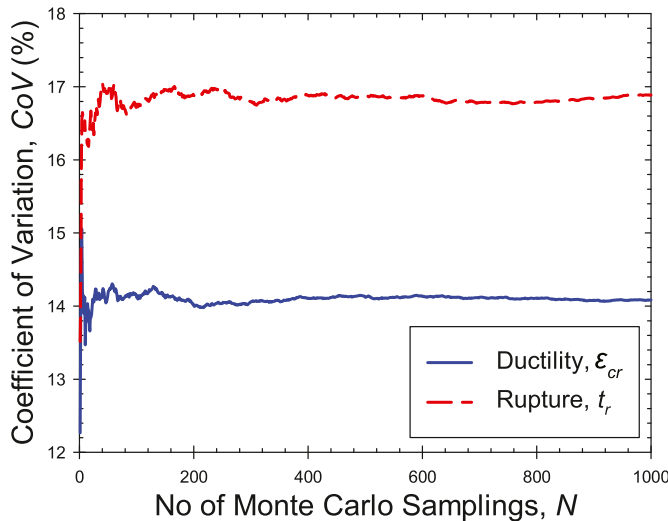


Fig. 8. The Coefficient of variation (CoV) convergence test of Monte Carlo Samplings for predicted creep ductility and rupture. Herein, the prediction at 320 MPa and 600 °C is employed.

sources in an assessment. The figure provides evidence that each uncertainty parameter contributes differently to the creep deformation curve. It should also be noted that changing the test conditions will change the relative effect of the parameters. It is observed that stress and initial damage alter all three results categories (MCSR, SR, and creep ductility). Temperature is missing an impact on creep ductility as previously described. The relative effects for MCSR data are deceptive as they are reported at the instant of load but in reality MCSR should be measured over the entire secondary creep regime (the linear portion of the creep curve). Following this logic, initial damage has the highest effect on the initial MCSR but little impact on the secondary creep regime as shown in Fig. 9(c) while stress has a much lower impact on the initial MCSR but a significant impact on secondary creep regime shown in Fig. 9(a). Neither λ nor φ influence the MCSR because initial damage is zero and λ does not contribute to SR because it does not exist in rupture [Eq. (12)].

5.5. Probabilistic predictions

The probabilistic model has all source of uncertainty “turned on”. Interpolative and extrapolative MCSR, SR, and creep deformation predictions are completed. The normalized MCSR and SR predictions are

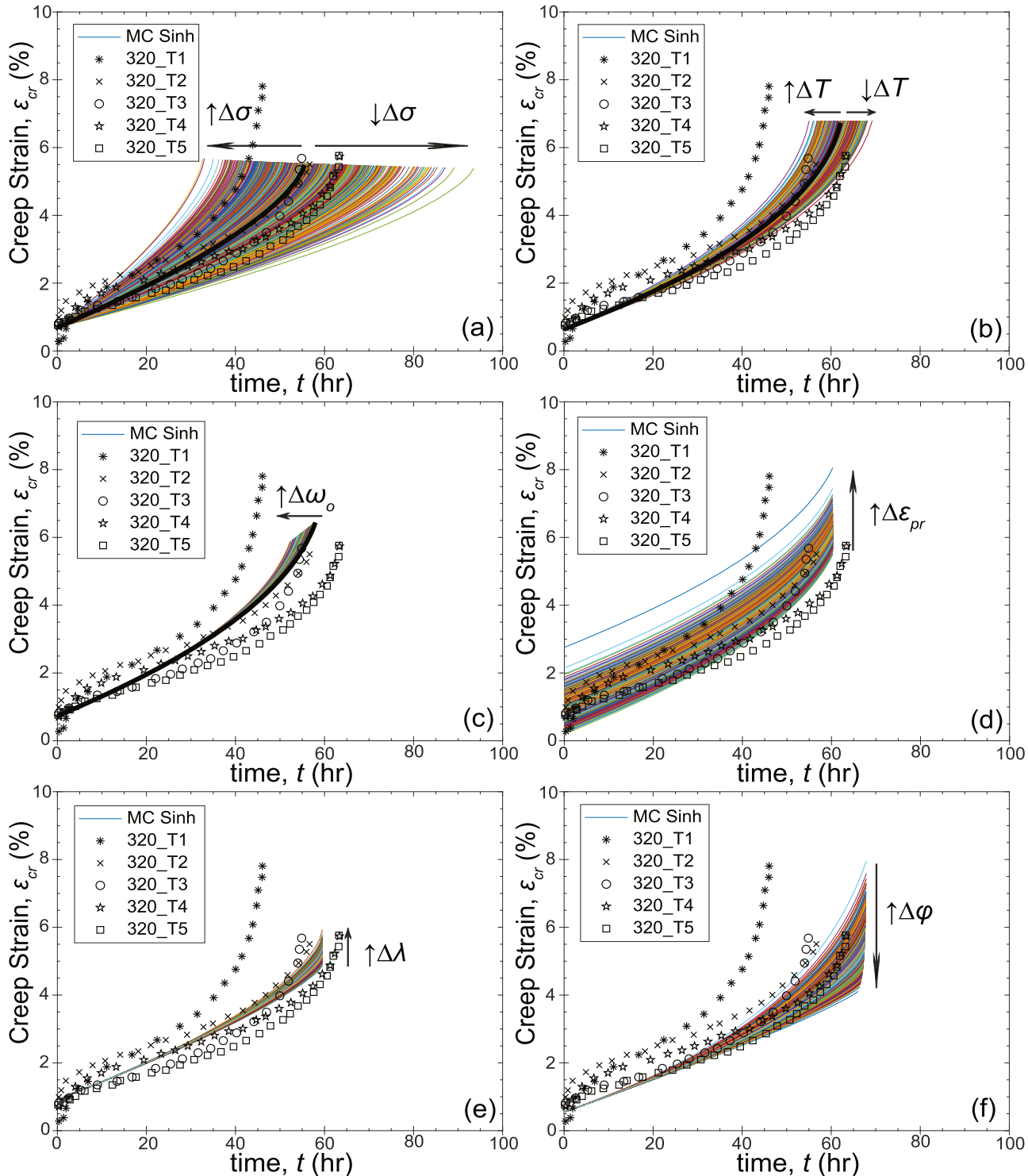


Fig. 9. Sensitivity analysis of creep deformation curves for (a) stress, σ (b) temperature, T (c) initial damage, ω_0 (d) primary creep, ε_{pr} (e) creep strain trajectory constant, λ , and (f) damage trajectory constant, φ uncertainty at 320 MPa and 600 °C. 1000 Monte Carlo simulations were performed for each source.

shown in Fig. 12(a) and (b), respectively. Qualitatively, the goodness-of-fit of the predictions are satisfactory. The model accurately predicts all isotherms with few outliers. The coefficient of determination (R^2) for normalized MCSR and SR is 0.798 and 0.976, respectively. In evaluating MCSR, the inclusion of uncertainty of the initial damage impacted the coefficient of determination (R^2) for predicted MCSR. The scatter of the MCSR and SR predictions increase with stress corresponding to the trend in the 304SS data. Different materials can exhibit different trends in

scatter depending on fundamental properties such as the processing and chemistry as well as the quantity and repeatability in the data available for calibration. For example, in a previous study, alloy 18Cr-8Ni was found to have a uniform scatter across stress while alloy 18Cr-12Ni-Mo exhibited an increasing scatter with decrease in stress [31]. The model shows flexibility in capturing these different trends in scatter via the Eyring's equation for λ and φ [Eqs. (7) and (8)] where the sign of the activation volume directs/inverts the relationship [51]. The variation of

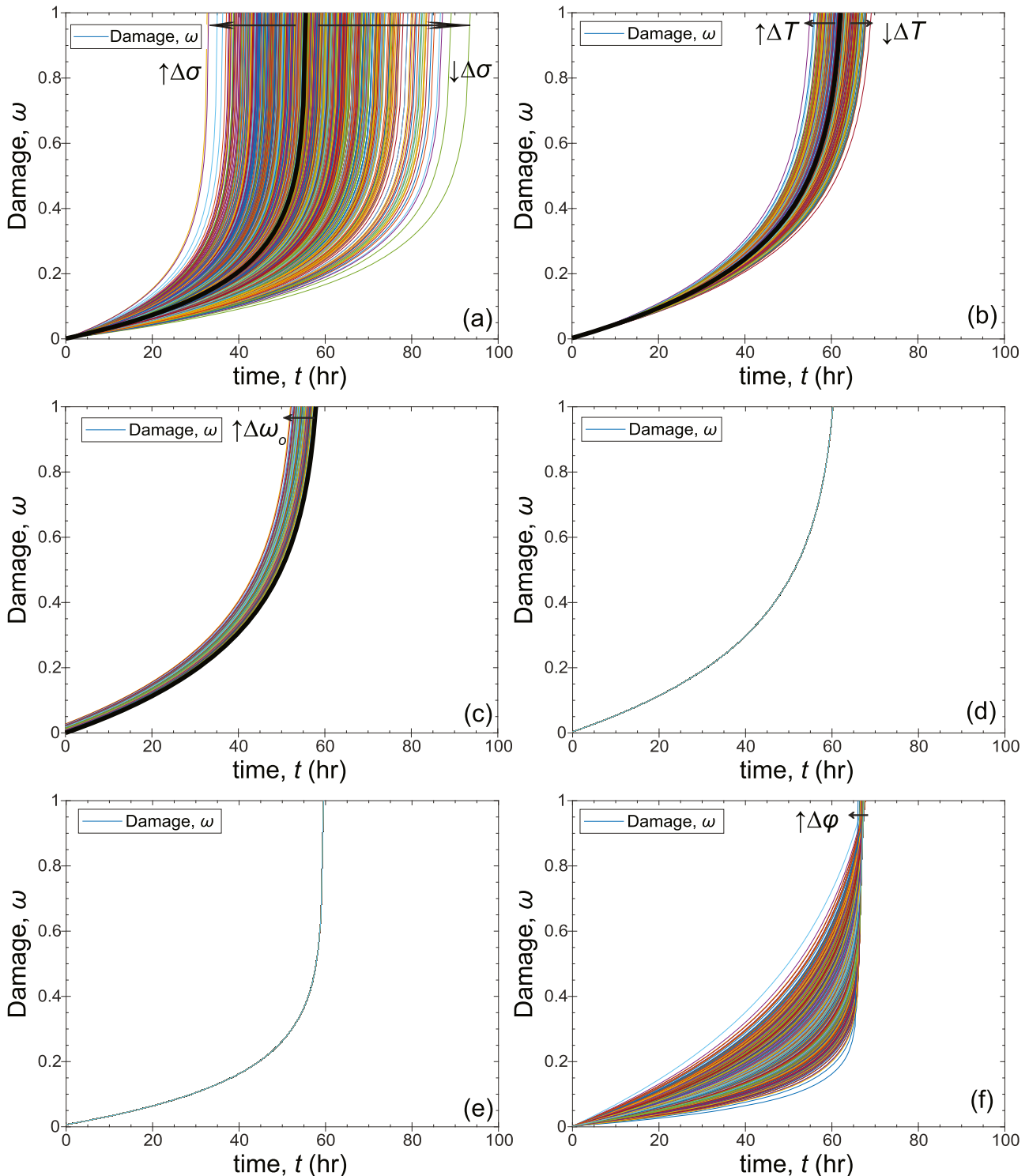


Fig. 10. Sensitivity analysis of damage evolution curves for (a) stress, σ (b) temperature, T (c) initial damage, ω_0 (d) primary creep, ε_{pr} (e) creep strain trajectory constant, λ , and (f) damage trajectory constant, φ uncertainty at 320 MPa and 600 °C. 1000 Monte Carlo simulations were performed for each source.

constants λ and φ cause the differing scatter bands in the aforementioned alloys.

To examine the scatter with respect to temperature, per isotherm predictions of MCSR and SR are provided in Fig. 13(a) and (b), respectively. The predicted scatter bands maintain a constant bandwidth across the isotherms. The uniform bandwidth is caused by the fixed standard deviation ($\mu = 4^\circ\text{C}/8$) employed in the pdf for temperature.

This behavior is consistent with the available experimental data, but bandwidth is observed to change with temperature in larger datasets for 304SS, 316SS, and other austenitic steels [31]. Using ASTM rules alone may not be sufficient to define temperature fluctuations during creep testing. A future study is needed to record and evaluate temperature fluctuations during creep testing and develop a more realistic probability distribution function. A key aspect to include may be the stochastic

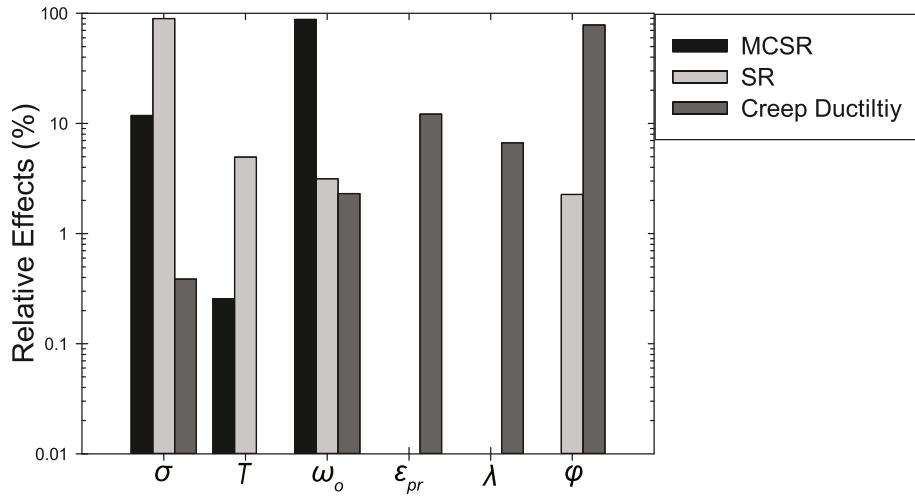


Fig. 11. Analysis of variance (ANOVA) of individual uncertainty parameters on MCSR, SR, and creep ductility prediction plotted as the relative effect on a log-scale. Results from the individual probabilistic predictions at 320 MPa and 600 °C are shown.

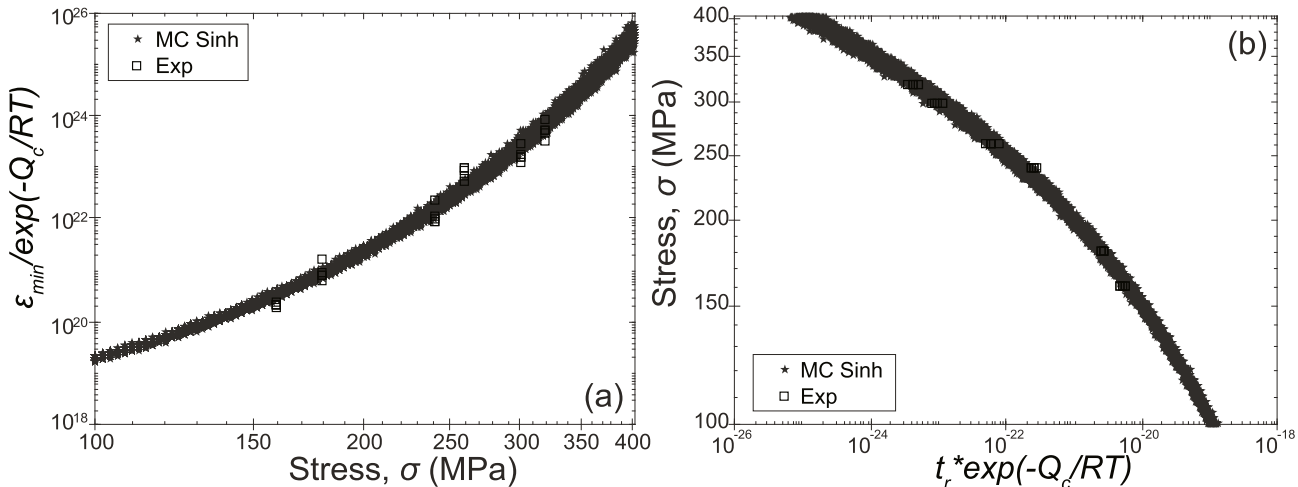


Fig. 12. Normalized (a) MCSR and (b) SR predictions using the full interaction model.

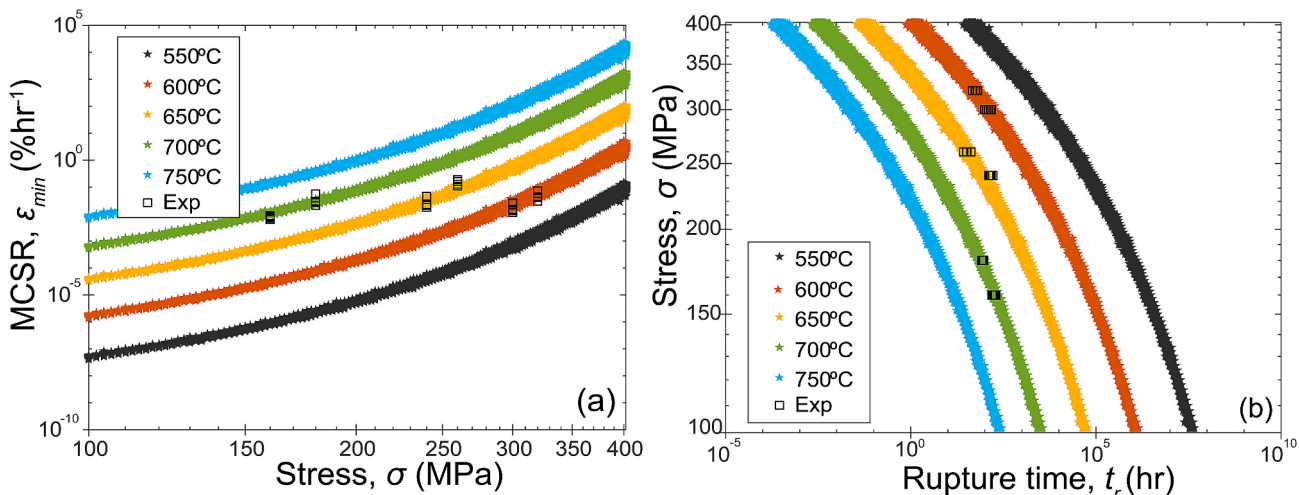


Fig. 13. Predicted (a) MCSR and (b) SR bands across multiple isotherms using the full interaction model. The bandwidth of the scatter bands remains unchanged as a function of temperature. The bandwidth decreases with stress.

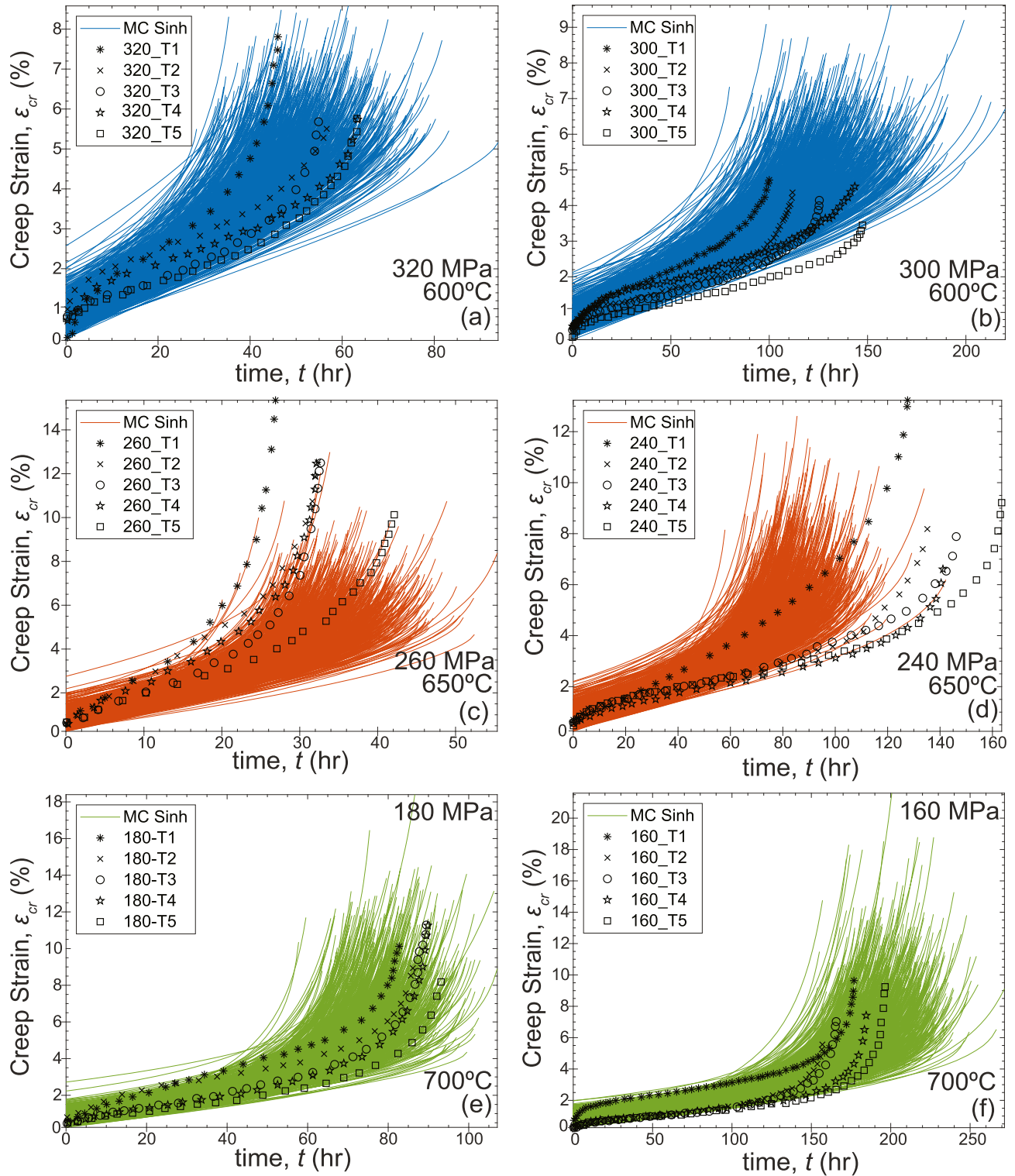


Fig. 14. Creep deformation curves using the full interaction model at 600 °C subjected to (a) 320 MPa and (b) 300 MPa, at 650 °C subjected to (c) 260 MPa and (d) 240 MPa, and at 700 °C subjected to (e) 180 MPa and (f) 160 MPa, respectively. Total Monte Carlo simulations per test condition is 1000.

behavior of temperature fluctuations as a function of time.

Creep deformation predictions of the experimental data are provided in Fig. 14(a)-(f). The goodness-of-fit of the predictions are satisfactory. The predictions at 650 °C are slightly offset from the experimental data but consistent with the outliers observed in the MCSR and SR predictions shown in Figs. 12 and 13.

The accuracy and precision statistics of the predictions are calculated

as follows

$$\text{Accuracy} = 100 \frac{|\bar{X}_{EXP} - \bar{X}_{SIM}|}{\bar{X}_{SIM}} \% \quad (15)$$

$$\text{Precision} = 100 \frac{SD_{SIM}}{\bar{X}_{SIM}} \% \quad (16)$$

Table 6

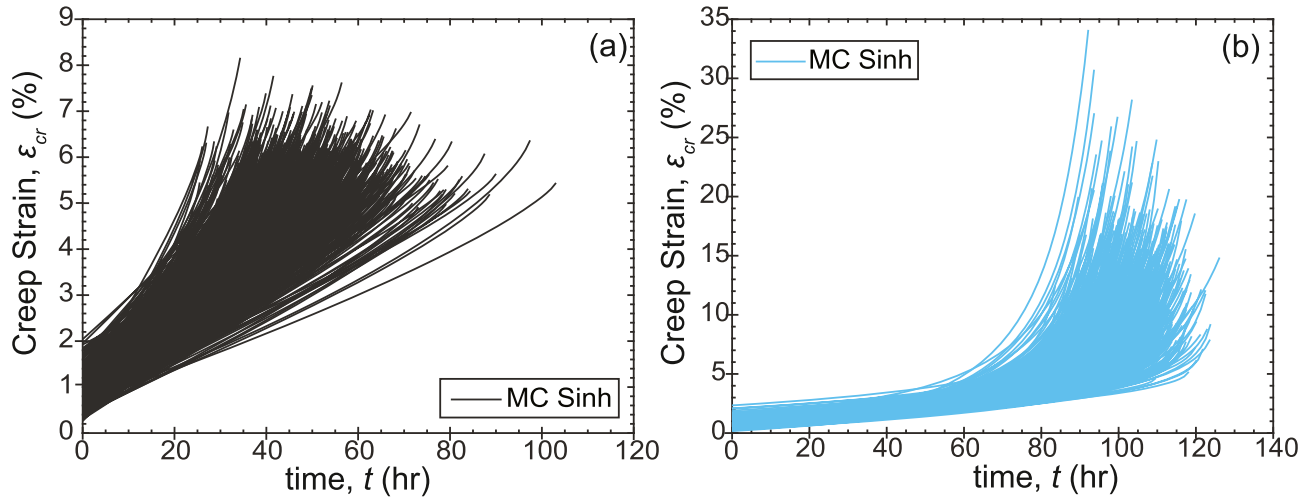
Accuracy and precision statistics of the predicted MCSR, SR, and creep ductility.

| Temperature, T (°C) | Stress, σ (MPa) | Accuracy | | | Precision | | |
|--------------------------|---------------------------|-------------|-----------|------------------|-------------|-----------|------------------|
| | | MCSR (%) | SR (%) | Ductility (%) | MCSR (%) | SR (%) | Ductility (%) |
| 600 | 320 | 55.874 | 4.755 | 3.531 | 70.244 | 16.887 | 14.086 |
| 600 | 300 | 61.780 | 5.489 | 27.825 | 79.268 | 16.066 | 15.504 |
| 650 | 260 | 7.777 | 6.668 | 96.022 | 99.742 | 14.274 | 19.634 |
| 650 | 240 | 61.961 | 62.180 | 36.989 | 101.365 | 13.406 | 21.112 |
| 700 | 180 | 63.127 | 10.485 | 23.152 | 148.246 | 10.101 | 26.139 |
| 700 | 160 | 80.851 | 11.674 | 9.771 | 153.429 | 9.279 | 26.994 |

< 10% - Good.

10%–50% - Acceptable.

>50% - Poor.

**Fig. 15.** Extrapolations of the creep deformation using the full interaction model at (a) 400 MPa and 550 °C and (b) 120 MPa and 750 °C, respectively.**Table 7**

Statistics of the predicted MCSR, SR, and creep ductility for Case A and B.

| Case Condition Type | A | | | B | | |
|---------------------------|-----------------------------------|------------|------------------|-----------------------------------|------------|------------------|
| | 400 MPa and 550 °C | | | 120 MPa and 750 °C | | |
| | MCSR (%. hr ⁻¹) | SR (hr) | Ductility (%) | MCSR (%. hr ⁻¹) | SR (hr) | Ductility (%) |
| Mean | 0.106 | 48.821 | 5.724 | 0.117 | 102.409 | 11.257 |
| Std Dev | 0.045 | 10.774 | 0.568 | 0.211 | 7.531 | 3.799 |
| Range | 0.480 | 77.589 | 4.555 | 1.943 | 44.262 | 29.671 |
| CoV | 42.919 | 22.068 | 9.928 | 180.954 | 7.353 | 33.753 |
| Upper 95% | 0.177 | 67.645 | 6.749 | 0.532 | 114.946 | 18.074 |
| CI | | | | | | |
| Lower 95% | 0.062 | 33.970 | 4.877 | 0.021 | 90.508 | 6.247 |
| CI | | | | | | |

where, SD_{SIM} is the standard deviation of the predictions, \bar{X}_{SIM} and \bar{X}_{EXP} are the respective mean of the predictions and experiments [52,53]. Perfect accuracy and precision are reported as 0%. The accuracy and precision statistics for MCSR, SR, and creep ductility predictions are summarized in Table 6. The accuracy and precision statistics <10% is considered as good, 10–50% as acceptable, and >50% as poor. This rationale will be used to determine the quality of the predictions, as predictions with good accuracy and precision will match experimental data closely. The accuracy correlates within acceptable range for SR and ductility except at test condition 240 and 260 MPa, respectively. The

precision statistics is observed to be free of significant outliers and demonstrate an affirmative trend with stress and temperature. Both accuracy and precision of MCSR correlates poorly. The MCSR statistics is projected to be poor with temperature. Overall, the probabilistic predictions show reasonable precision with acceptable accuracy when compared to the experimental data.

The extrapolation ability of the probabilistic model is evaluated by performing simulations outside of the available data. Two extremes conditions are considered a) high-stress and low-temperature at 400 MPa and 550 °C and b) low-stress and high-temperature at 120 MPa and 750 °C as shown in Fig. 15. The MCSR, SR, and creep ductility statistics are summarized in Table 7. Case A exhibits a larger CoV in SR which is consistent with the trend observed in the available data. Case B exhibits a larger CoV in MCSR and creep ductility which is expected where the low-stress allows for more variation in the MCSR, secondary creep regime, and subsequently the creep ductility.

5.6. Discussion

The probabilistic creep model is shown to be a promising approach for dealing with uncertainty in test conditions, damage, and material properties in materials subjected to creep. A number of observations can be made concerning the model's limitations and areas for improvement.

The model was calibrated using quintuplicate creep deformation curves. A much larger quantity of replicate data would greatly improve the model's probabilistic predictions; however, it may not be reasonable due to the high cost of creep testing. As an alternative, the disparate data approach can be employed where available creep deformation curves

are enhanced with legacy datasets of MCSR, SR, and creep ductility [29]. Note, when using legacy datasets (e.g. NIMS Material database), the chemical composition and heat treatment must be carefully examined to avoid exaggerated uncertainty due to the possibility of deleterious phases and particulate particles [54].

The temperature record and eccentricity measurements were not available in this study. This data is rarely preserved during conventional creep testing. These measurements are critically important, as they calibrate the test condition pdfs and feed into the initial damage pdf. Such data is cheaply acquired and is recommended for future investigations. Additionally, the co-calibration of the sources of uncertainty as opposed to piecewise calibration should be investigated further.

Post-audit validation should be performed, where data not used in calibration is compared to simulations, to provide a quantitative measure of extrapolation ability. The small dataset available here $N = 30$, prevented such an analysis from being performed.

Deformation mechanisms are a function of stress and temperature. A change in deformation mechanism can cause a change in creep activation energy and material properties. Deformation mechanism maps should be consulted when calibrating the model, as mechanism transition will also shift the material property pdfs.

Stochasticity exists in material properties where uncertainty is not fixed; rather, expands with time. Metallurgical changes (phase transformations, carbide precipitation and coarsening, etc.) dominate at low life fractions, requiring time and temperature to nucleate. When new phases nucleate, a change in creep resistance can occur shifting both the magnitude and uncertainty of material properties. Time-temperature-transformation (TTT) and -precipitation (TP) diagrams (whether experimental or calculated) should be consulted to identify regions of interests. Stochastic pdfs are needed to account for these time-dependent behaviors.

Based on these observations, the accuracy, precision, and extrapolation ability of the model can be improved by conducting more tests over a wide range of test conditions, recording more information per test, setting aside a post-audit validation dataset, and consulting deformation mechanism, TTT, and TP diagrams. The probabilistic model employed in this study utilizes the short-term data to extrapolate up to 10^6 hr of creep data as shown in Fig. 13. A more extensive dataset of austenitic stainless steels gathered from NIMS is used to examine the model's extrapolation ability [31,55]. Future work will focus on these areas for improvement.

6. Conclusion

The objective of this study was to develop a probabilistic Sinh model to predict the uncertainty of creep deformation, damage, and rupture in alloys. Probabilistic predictions of alloy 304SS were analyzed and have led to the following insights:

APPENDIX

Table 8

Specimen-specific material constant for Sinh model with alloy 304SS.

| Test ID | Stress, σ | ε_{pr} | A^* | M^* | λ | φ | $\dot{\varepsilon}_{min}$ | Rupture time, t_r |
|---------|------------------|--------------------|-------|-------|-----------|-----------|---------------------------|---------------------|
| | | | | | | | | |
| 600 °C | | | | | | | | |
| 320_T1 | 320 | 0.85 | 4.12 | 10.89 | 3.16 | 6.97 | 0.073 | 46.05 |
| 320_T2 | 320 | 1.45 | 2.49 | 8.85 | 1.59 | 5.04 | 0.044 | 56.64 |
| 320_T3 | 320 | 0.76 | 2.42 | 9.14 | 3.04 | 6.59 | 0.043 | 54.87 |
| 320_T4 | 320 | 1.20 | 2.33 | 7.91 | 1.85 | 6.07 | 0.041 | 63.36 |
| 320_T5 | 320 | 0.82 | 1.68 | 7.93 | 2.46 | 3.39 | 0.029 | 63.23 |
| 300_T1 | 300 | 0.80 | 3.75 | 12.37 | 2.09 | 9.04 | 0.025 | 100.00 |
| 300_T2 | 300 | 0.82 | 2.11 | 11.05 | 2.72 | 5.49 | 0.014 | 111.86 |

(continued on next page)

- Deterministic predictions of the MCSR, SR, and creep ductility show satisfactory agreement with the experimental data.
- Sensitivity analysis revealed the differing contributions of the uncertainty parameter to creep resistance. The contributions arise from the interferences of the model equations, assigned pdfs, and are a function of stress and temperature.
- The probabilistic MCSR, SR, and creep deformation predictions are reasonably accurate and precise across multiple isotherms with a few outliers. The predicted MCSR, SR, and creep ductility are observed to be more precise with an acceptable level of accuracy.
- A larger dataset is needed if extrapolative predictions are to be achieved. Overall, the probabilistic model is good for interpolation but lacks in extrapolation ability.

The proposed future investigations can further improve the probabilistic model.

Author statement

Md Abir Hossain: Methodology, Investigation, Simulation, Writing original draft, Data visualization, Review and Editing. **Calvin M Stewart:** Conceptualization, Writing, Review and Editing, Supervision, Project administration.

Declaration of competing interest

The authors declare that they have no known competing financial interests or personal relationships that could have appeared to influence the work reported in this paper.

Acknowledgement

This research was funded by the Department of Energy, National Energy Technology Laboratory under award number DE-FE0027581, which is greatly acknowledged.

This report was prepared as an account of work sponsored by an agency of the United States Government. Neither the United States Government nor any agency thereof, nor any of their employees, makes any warranty, express or implied, or assumes any legal liability or responsibility for the accuracy, completeness, or usefulness of any information, apparatus, product, or process disclosed, or represents that its use would not infringe privately owned rights. Reference herein to any specific commercial product, process, or service by trade name, trademark, manufacturer, or otherwise does not necessarily constitute or imply its endorsement, recommendation, or favoring by the United States Government or any agency thereof. The views and opinions of authors expressed herein do not necessarily state or reflect those of the United States Government or any agency thereof.

Table 8 (continued)

| Test ID | Stress, σ | ε_{pr} | A* | M* | λ | φ | $\dot{\varepsilon}_{min}$ | Rupture time, t_r |
|---------------|------------------|--------------------|----------------------------|--------------------------|-----------|-----------|---------------------------|---------------------|
| | MPa | % | $\%hr^{-1} \times 10^{17}$ | $hr^{-1} \times 10^{17}$ | | | $\%hr^{-1}$ | hr |
| 300_T3 | 300 | 0.73 | 1.96 | 9.85 | 3.39 | 8.19 | 0.013 | 125.48 |
| 300_T4 | 300 | 0.95 | 2.20 | 8.61 | 1.47 | 4.19 | 0.015 | 143.52 |
| 300_T5 | 300 | 0.63 | 1.65 | 8.39 | 2.25 | 7.09 | 0.011 | 147.43 |
| 650 °C | | | | | | | | |
| 260_T1 | 260 | 0.45 | 8.05 | 12.28 | 2.53 | 3.30 | 0.046 | 26.88 |
| 260_T2 | 260 | 1.05 | 8.10 | 10.21 | 2.05 | 4.58 | 0.017 | 32.31 |
| 260_T3 | 260 | 0.83 | 5.44 | 10.10 | 2.79 | 3.87 | 0.022 | 32.67 |
| 260_T4 | 260 | 0.70 | 6.89 | 10.27 | 3.25 | 6.40 | 0.020 | 32.14 |
| 260_T5 | 260 | 1.00 | 4.66 | 7.83 | 2.12 | 4.16 | 0.017 | 42.12 |
| 240_T1 | 240 | 0.70 | 5.14 | 6.38 | 2.57 | 4.86 | 0.187 | 127.61 |
| 240_T2 | 240 | 0.55 | 1.98 | 6.02 | 2.37 | 2.82 | 0.188 | 135.14 |
| 240_T3 | 240 | 0.50 | 2.51 | 5.57 | 2.03 | 3.98 | 0.126 | 146.18 |
| 240_T4 | 240 | 0.70 | 2.32 | 5.77 | 2.25 | 5.69 | 0.160 | 141.10 |
| 240_T5 | 240 | 0.65 | 1.96 | 4.98 | 2.96 | 4.41 | 0.108 | 163.52 |
| 700 °C | | | | | | | | |
| 180_T1 | 180 | 0.90 | 6.61 | 9.03 | 2.21 | 5.31 | 0.056 | 82.73 |
| 180_T2 | 180 | 1.55 | 3.25 | 8.67 | 2.78 | 3.43 | 0.027 | 86.14 |
| 180_T3 | 180 | 0.43 | 3.52 | 8.35 | 3.55 | 3.73 | 0.030 | 89.48 |
| 180_T4 | 180 | 0.65 | 3.11 | 8.31 | 3.80 | 3.95 | 0.026 | 89.83 |
| 180_T5 | 180 | 0.60 | 2.42 | 8.02 | 3.05 | 2.99 | 0.020 | 93.12 |
| 160_T1 | 160 | 1.45 | 2.67 | 10.52 | 4.55 | 4.41 | 0.008 | 176.84 |
| 160_T2 | 160 | 0.42 | 2.43 | 11.86 | 3.84 | 4.19 | 0.007 | 156.95 |
| 160_T3 | 160 | 0.41 | 2.26 | 11.24 | 4.39 | 4.24 | 0.007 | 165.63 |
| 160_T4 | 160 | 0.56 | 2.14 | 10.09 | 4.09 | 4.09 | 0.007 | 184.51 |
| 160_T5 | 160 | 0.45 | 1.90 | 9.47 | 5.02 | 4.50 | 0.006 | 196.41 |

References

- [1] A. Vojdani, G.H. Farrahi, A. Mehmanparast, B. Wang, Probabilistic assessment of creep-fatigue crack propagation in austenitic stainless steel cracked plates, Eng. Fract. Mech. 200 (2018) 50–63, <https://doi.org/10.1016/j.engfracmech.2018.07.022>.
- [2] H. Mao, S. Mahadevan, Reliability analysis of creep-fatigue failure, Int. J. Fatig. 22 (2000) 789–797, [https://doi.org/10.1016/S0142-1123\(00\)00046-3](https://doi.org/10.1016/S0142-1123(00)00046-3).
- [3] R.B. Davies, R. Hales, J.C. Harman, S.R. Holdsworth, Statistical modeling of creep rupture data, J. Eng. Mater. Technol. Trans. ASME. 121 (1999) 264–271.
- [4] N.A. Zentuti, J.D. Booker, R.A.W. Bradford, C.E. Truman, Correlations between creep parameters and application to probabilistic damage assessments, Int. J. Pres. Ves. Pip. 165 (2018) 295–305, <https://doi.org/10.1016/j.ijpvp.2018.07.004>.
- [5] F. Garofalo, R.W. Whittemore, W.F. Domis, F. Vongemmingen, Creep and creep-rupture relationships in an austenitic stainless-steel, Trans. Metallurgical Soc. AIME. 221 (1961) 310–319.
- [6] M. Evans, A statistical analysis of the failure time distribution for $\%Cr/\%Mo/\%V$ steel tubes in the presence of outliers, Int. J. Pres. Pip. 60 (1994) 193–207.
- [7] W. Rutman, M. Krause, K.J. Kremer, International community tests on long-term behavior of 2 1 4 Cr-1 Mo steel, in: Proc. Joint. Conf. High-Temperature Prop. Steels, 1966, pp. 232–239.
- [8] M.K. Booker, B.L.P. Booker, R.W. Swindeman, Analysis of Elevated-Temperature Tensile and Creep Properties of Normalized and Tempered 2-1/4Cr-1Mo Steel, Oak Ridge National Lab, TN (USA), 1982.
- [9] S.J. Kim, Y.S. Kong, Y.J. Roh, W.G. Kim, Statistical properties of creep rupture data distribution for STS304 stainless steels, Mater. Sci. Eng. 483–484 (2008) 529–532, <https://doi.org/10.1016/j.msea.2006.12.153>.
- [10] D.G. Harlow, T.J. Delph, Creep deformation and failure: effects of randomness and scatter, J. Eng. Mater. Technol. Trans. ASME. 122 (2000) 342–347, <https://doi.org/10.1115/1.482807>.
- [11] D.R. Hayhurst, The effects of test variables on scatter in high-temperature tensile creep-rupture data, Int. J. Mech. Sci. 16 (1974) 829–841.
- [12] J.P. Farris, J.D. Lee, D.G. Harlow, T.J. Delph, On the scatter in creep rupture times, Metall. Trans. A. 21 (1990) 345–352, <https://doi.org/10.1007/BF02782414>.
- [13] G. Eggeler, Microstructural parameters for creep damage quantification, Acta Metall. Mater. 39 (1991) 221–231.
- [14] M.S. Haque, C.M. Stewart, Modeling the creep deformation, damage, and rupture of hastelloy X using MPC Omega, Theta, and sine-hyperbolic models, in: Proc. ASME 2016 Press. Vessel. Pip. Conf. PVP 2016, British Columbia, Canada, Vancouver, 2016, pp. 1–10.
- [15] M.S. Haque, C.M. Stewart, Exploiting functional relationships between MPC Omega, Theta, and sine-hyperbolic continuum damage mechanics model, in: Proc. ASME 2016 Press. Vessel. Pip. Conf. PVP 2016, British Columbia, Canada, Vancouver, 2016, pp. 1–11.
- [16] J.A. Cano, C.M. Stewart, Application of the Wilshire stress-rupture and minimum-creep-strain-rate prediction models for alloys P91 in tube, plate, and pipe form, in: Proc. ASME Turbo Expo 2019 Turbomach, Tech. Conf. Expo. GT2019, Phoenix, Arizona, USA, 2019.
- [17] J. Perez, C.M. Stewart, Assessment of the Theta projection model for interpolating creep deformation, in: Proc. ASME Turbo Expo 2019 Turbomach, Tech. Conf. Expo. GT2019, Phoenix, Arizona, USA, 2019.
- [18] Y. Appalanaidu, Y. Vyasa, S. Gupta, Stochastic creep damage growth due to random thermal fluctuations using continuum damage mechanics, Procedia Eng 55 (2013) 805–811, <https://doi.org/10.1016/j.proeng.2013.03.335>.
- [19] D.G. Harlow, T.J. Delph, A computational probabilistic model for creep-damaging solids, Comput. Struct. 54 (1995) 161–166.
- [20] M.A. Hossain, C.M. Stewart, Reliability prediction of 304 stainless steel using sine-hyperbolic creep-damage model with Monte Carlo simulation method, in: Proc. ASME 2019 Press. Vessel Pip. Conf. PVP2019, San Antonio, Texas, USA, 2019.
- [21] Y. Appalanaidu, A. Roy, S. Gupta, Stochastic creep damage estimation in piping with spatial non-Gaussian uncertainties using spectral stochastic finite element method, Procedia Eng 86 (2014) 677–684, <https://doi.org/10.1016/j.proeng.2014.11.069>.
- [22] W.G. Kim, J.Y. Park, S.D. Hong, S.J. Kim, Probabilistic assessment of creep crack growth rate for Gr. 91 steel, Nucl. Eng. Des. 241 (2011) 3580–3586, <https://doi.org/10.1016/j.nucengdes.2011.06.042>.
- [23] R.K. Penny, M.A. Weber, Robust methods of life assessment during creep, Int. J. Pres. Ves. Pip. 50 (1992) 109–131, [https://doi.org/10.1016/0308-0161\(92\)90033-C](https://doi.org/10.1016/0308-0161(92)90033-C).
- [24] B. Bhattacharya, B. Ellingwood, Continuum damage mechanics-based model of stochastic damage growth, J. Eng. Mech. 124 (1998) 1000–1009.
- [25] W.G. Kim, J.Y. Park, S.J. Kim, J. Jang, Reliability assessment of creep rupture life for Gr. 91 steel, J. Mater. Des. 51 (2013) 1045–1051, <https://doi.org/10.1016/j.matedes.2013.05.013>.
- [26] J. Zhao, D. ming Li, J. shan Zhang, W. Feng, Y. yuan Fang, Introduction of SCRI model for creep rupture life assessment, Int. J. Pres. Ves. Pip. 86 (2009) 599–603, <https://doi.org/10.1016/j.ijpvp.2009.04.004>.
- [27] C.M. Stewart, A Hybrid Constitutive Model for Creep, Fatigue, and Creep-Fatigue Damage, University of Central Florida, 2013.
- [28] M.S. Haque, C.M. Stewart, The stress-sensitivity, mesh-dependence, and convergence of continuum damage mechanics models for creep, J. Press. Vessel Technol. Trans. ASME. 139 (2017) 1–10, <https://doi.org/10.1115/1.4036142>.
- [29] M.S. Haque, C.M. Stewart, The disparate data problem: the calibration of creep laws across test type and stress, temperature, and time scales, Theor. Appl. Fract. Mech. 100 (2019) 251–268.
- [30] M.S. Haque, C.M. Stewart, Finite-element analysis of waspaloy using Sinh creep-damage constitutive model under triaxial stress state, J. Press. Vessel Technol. Trans. ASME 138 (3) (2016) 1–9.
- [31] M.A. Hossain, C.M. Stewart, Probabilistic minimum-creep-strain-rate and stress-rupture for the long-term assessment of IGT components, in: Proc. ASME Turbo Expo 2020 Turbomach, Tech. Conf. Expo. GT2020, London, England, 2020.
- [32] E. Liebscher, Approximation of distributions by using the Anderson Darling statistic, Commun. Stat. Theor. Methods 45 (2016) 6732–6745, <https://doi.org/10.1080/03610926.2014.966844>.
- [33] B.Y. Lemeshko, I.V. Veretennikova, S.B. Lemeshko, A.Y. Novikova, in: V. V Rykov, N.D. Singpurwalla, A.M. Zubkov (Eds.), Application of Homogeneity Tests:

- Problems and Solution BT - Analytical and Computational Methods in Probability Theory, Springer International Publishing, Cham, 2017, pp. 461–475.
- [34] A.K. Sharma, Text Book of Correlations and Regression, Discovery Publishing House, 2005.
- [35] M. Hadid, B. Guerira, M. Bahri, A. Zouani, Assessment of the stepped isostress method in the prediction of long term creep of thermoplastics, *Polym. Test.* 34 (2014) 113–119.
- [36] A.D. Drozdov, Creep rupture and visco elastoplasticity of polypropylene, *Eng. Fract. Mech.* 77 (2010) 2277–2293.
- [37] A.S. for T. and M. (ASTM), ASTM E139-11. Standard Test Methods for Conducting Creep, Creep-Rupture, and Stress-Rupture Tests of Metallic Materials, 2011.
- [38] A. Miller, An inelastic constitutive model for monotonic, cyclic, and creep deformation: Part II—application to type 304 stainless steel, *J. Eng. Mater. Technol. Trans. ASME.* 98 (1976) 106–112, <https://doi.org/10.1115/1.3443346>.
- [39] A.S.T.M., Standard, E8. Standard Test Method for Tension Testing of Metallic Materials, West Conshohocken ASTM, 2004.
- [40] B.F. Dyson, D. McLean, A new method of predicting creep life, *Met. Sci. J.* 6 (1972) 220–223, <https://doi.org/10.1179/030634572790446181>.
- [41] C.J. Middleton, Reheat cavity nucleation and nucleation control in bainitic creep-resisting low-alloy steels: roles of manganese sulphide, residual, and Sulphur-stabilizing elements, *Met. Sci.* 15 (1981) 154–167.
- [42] D. Bae, A.K. Ghosh, Cavity formation and early growth in a superplastic Al-Mg alloy, *Acta Mater.* 50 (2002) 511–523.
- [43] N.G. Needham, T. Gladman, Nucleation and growth of creep cavities in a Type 347 steel, *Met. Sci.* 14 (1980) 64–72, <https://doi.org/10.1179/030634580790426300>.
- [44] C. Gupta, H. Toda, C. Schlacher, Y. Adachi, P. Mayr, C. Sommitsch, K. Uesugi, Study of creep cavitation behavior in tempered martensitic steel using synchrotron micro-tomography and serial sectioning techniques, *Mater. Sci. Eng.* 564 (2013) 525–538, <https://doi.org/10.1016/j.msea.2012.12.002>.
- [45] J. Kar, S. Kumar, G. Gopal, S. Kumar, X-ray tomography study on porosity in electron beam welded dissimilar copper e 304SS joints, *Vaccum* 149 (2018) 200–206, <https://doi.org/10.1016/j.vacuum.2017.12.038>.
- [46] J.A. Slotwinski, E.J. Garboczi, K.M. Hebenstreit, Porosity measurement and analysis for metal additive manufacturing process control, *J. Res. Natl. Inst. Stand. Technol.* 119 (2014) 494–528, <https://doi.org/10.6028/jres.119.019>.
- [47] C.M. Stewart, A.P. Gordon, Constitutive modeling of multistage creep damage in isotropic and transversely isotropic alloys with elastic damage, *J. Pressure Vessel Technol.* 134 (2012), <https://doi.org/10.1115/1.4005946>.
- [48] T. Pang, Y. Yang, D. Zhao, Convergence studies on Monte Carlo methods for pricing mortgage-backed securities, *Int. J. Financ. Stud.* 3 (2015) 136–150, <https://doi.org/10.3390/ijfs3020136>.
- [49] R. Viswanathan, Damage Mechanisms and Life Assessment of High Temperature Components, ASM international, 1989.
- [50] R. Viswanathan, Effect of stress and temperature on the creep and rupture behavior of a 1.25 Pct chromium—0.5 Pct molybdenum steel, *Metall. Trans. A.* 8 (1977) 877–884.
- [51] O.D. Sherby, J.L. Robbins, A. Goldberg, Calculation of activation volumes for self-diffusion and creep at high temperature, *J. Appl. Phys.* 41 (1970) 3961–3968.
- [52] R.C. Foster, L.M. Lanningham-Foster, C. Manohar, S.K. McCrady, L.J. Nysse, K. R. Kaufman, D.J. Padgett, J.A. Levine, Precision and accuracy of an ankle-worn accelerometer-based pedometer in step counting and energy expenditure, *Prev. Med.* 41 (3–4) (2005) 778–783.
- [53] S. Rekolainen, M. Posch, J. Kämäri, P. Ekholm, Evaluation of the accuracy and precision of annual phosphorus load estimates from two agricultural basins in Finland, *J. Hydrol.* 128 (1–4) (1991) 237–255.
- [54] Creep Data Sheet(CDS) - DICE :: National Institute for Materials Science (nims.go.jp).
- [55] M.A. Hossain. A Probabilistic Creep Constitutive Model for Creep Deformation, Damage, and Rupture, The University of Texas at El Paso, 2020. <http://0-search.proquest.com.lib.utep.edu/dissertations-theses/probabilistic-creep-constitutive-model/docview/2455534563/se-2?accountid=7121>.